A Lens Array Multi-beam MIMO Testbed for Real-Time mmWave Communication and Sensing

Akbar Sayeed
University of Wisconsin-Madison
Madison, WI
akbar.sayeed@wisc.edu

Christopher Hall
University of Wisconsin-Madison
Madison, WI
chall24@wisc.edu

Kevin (Yifan) Zhu
University of Wisconsin
Madison, WI
zhu273@wisc.edu

ABSTRACT

Millimeter-wave (mmW) wireless is a promising technology for meeting the Gigabit rate and millisecond latency requirements of emerging applications. This promise fundamentally rests on the large (GHz) bandwidths and high-gain/high-dimensional beamforming possible at mmW frequencies. While multi-beam multiple input multiple output (MIMO) operation is necessary for achieving spatial multiplexing, existing systems are limited to mechanically pointed horn antennas and single-beam phased arrays of moderate sizes. In this paper, we report the development of a new testbed architecture for multi-beam MIMO communication and sensing at mmW frequencies. The testbed uses a novel lens array for multi-beamforming and data multiplexing. The paper provides a brief overview of the underlying beamspace MIMO framework, and presents initial measurement results to illustrate three key testbed functionalities: directional communication through the lens array; multiuser commmunication; and analysis of the measurement data, including channel measurements.

CCS CONCEPTS

• **Hardware → Communication hardware, interfaces and storage**; **Digital signal processing**; **Beamforming**; **Emerging technologies**; **Analysis and design of emerging devices and systems**; **Emerging architectures**; **Emerging tools and methodologies**;

KEYWORDS

Millimeter-Wave; Prototype; Beamforming; Channel Measurements; MIMO; FPGA; Lens Array

1 INTRODUCTION

The large bandwidths and narrow beamwidths afforded by millimeter wave (mmW) wireless systems represent a promising opportunity for meeting the growing data rate requirements through high-dimensional MIMO operation [6, 9, 10, 18]. The large number of MIMO degrees of freedom can be exploited for a number of critical capabilities including: higher beamforming gain; higher spatial multiplexing gain; and highly directional communication with narrow beams. The multiplexing gain of conventional MIMO systems depends heavily on the richness of multipath propagation [5, 16]. On the other hand, spatial multiplexing is achieved at mmW through multiuser point-to-multipoint operation over narrow beams, and primarily over a sparse set of line-of-sight (LoS) and/or single-bounce multipath propagation paths [6]. Furthermore, agile beam steering is needed in mobile environments to circumvent the higher probability of blockage at mmW frequencies. As a result, agile multi-beamforming and data multiplexing is a key operational functionality in mmW wireless, and beamspace system modeling is naturally applicable [2, 11, 13].

In this paper, we present initial results on a new mmW MIMO wireless testbed that leverages a state-of-the-art multi-beam MIMO transceiver architecture, called continuous aperture phased (CAP)-MIMO, proposed by our group [2, 11]. A CAP-MIMO transceiver performs analog multi-beamforming using a lens antenna array and offers a new methodology for beamspace MIMO communication and sensing. We have recently completed the construction of a 28 GHz CAP-MIMO prototype that is capable of simultaneously transmitting or receiving on four spatial channels by electronically selecting 4 out of 16 beams [3]. This paper builds on initial results on line-of-sight (LoS) pathloss measurements in [14] and multipath channel measurements in [12].

All existing prototype mmW systems rely on phased arrays for beamforming which are limited to a single beam per array aperture, requiring multiple arrays for multiple beams. Similarly, there has been significant recent work on mmW channel modeling and measurements at frequencies ranging from 28GHz to 73GHz; see, e.g. [7, 8, 17]. However, these works are based on mechanically pointed horn antennas or single-beam phased arrays. The lens array-based CAP-MIMO testbed reported in this work is capable of multi-beamforming and spatial resolutions not possible with existing systems. Sec. 2 provides a description of the 28GHz CAP-MIMO prototype. A brief review of beamspace MIMO framework is presented in Sec. 3, followed by the new results in Sec. 5. Concluding remarks are provided in Sec. 6.

2 CAP-MIMO TESTBED DESCRIPTION

The 28GHz prototype testbed system consists of a CAP-MIMO access point (AP) communicating with multiple single-antenna mobile stations (MSs) as shown in Fig. 1(a). The CAP-MIMO transceiver at the AP uses a 6" circular lens with a 16-feed square (4×4) array of antennas on its focal surface representing $N_b = 16$ distinct beams; see Fig. 1(b). The CAP-MIMO AP can simultaneous transmit or receive $p = 4$ signals from the 16-feed array through $p = 4$ transmit/receive (T/R) mmW chains, as shown in Fig. 1(c). Each MS

mmNets'17, October 17, 2017, Snowbird, UT, USA

ACM ISBN 978-1-4503-5143-0/17/10…$15.00
https://doi.org/10.1145/3130242.3131488

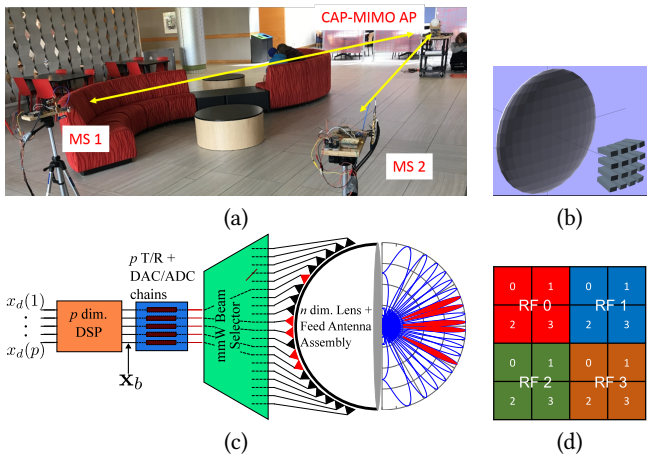

Figure 1: (a) A 28GHz CAP-MIMO prototype testbed link. (b) A 16-feed lens array used in the prototype. (c) A CAP-MIMO transceiver schematic. (d) Beams associated with each of the four channels.

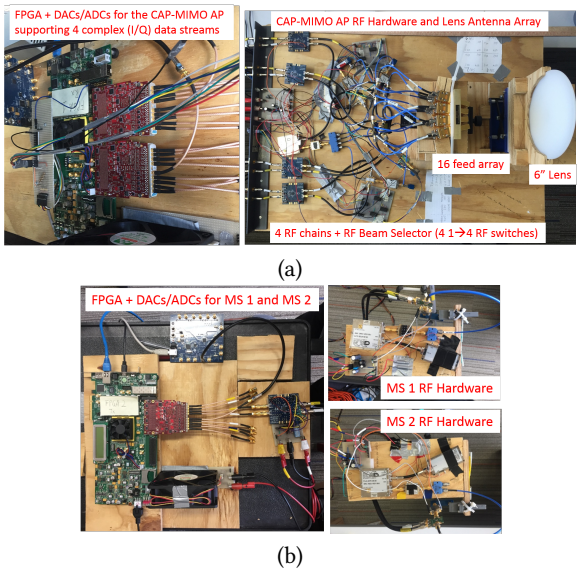

Figure 2: CAP-MIMO prototype testbed hardware, including antennas, mmW hardware, data convertors, and FPGA-based BPU. (a) A CAP-MIMO AP node with a lens array and supporting four channels. (b) Single channel MS nodes with waveguide antennas.

transceiver is equipped with a single mmW T/R chain. The feed antennas at the AP and the MS antenna are open-ended WR-28 waveguides. Each mmW T/R chain (at the AP or MS) consists of a highly stable local oscillator (LO), an I/Q mixer (IQM), a power amplifier with 16 dB gain or a low-noise amplifier with 23 dB gain, and a bandpass filter. Each mmW T/R chain has a bandwidth of 1 GHz centered at 28 GHz. All IQMs are driven by the same LO at the AP receiver. At the CAP-MIMO AP receiver, four beams can be simultaneously measured, one in each quadrant of 4 feeds; see Fig. 1(d). Each mmW measurement chain can be switched to one of the beams in each quadrant using a 1-to-4 mmW switch.

The AP is connected to a baseband processing unit (BPU) consisting of a Xilinx VC707 FPGA board populated with two FMC144 data convertor cards from 4DSP, each supporting four 16-bit ADC channels operating at 370MS/s and four 16-bit DAC channels with peak sampling rate of 2.5GS/s to support up to 4x oversampling for pulse shaping. Thus, the current testbed supports a communication bandwidth of $W = 370$MHz. For the results reported in this paper, the AP is configured as a receiver and the MSs serve as transmitters. Both the MSs are supported by a single VC707 board for baseband processing. Both FPGAs boards are connected to their own host PCs for running MATLAB scripts that are used for configuring the transmission frame for the MSs, measurements at the CAP-MIMO AP, and data extraction from the AP FPGA board.

Photographs of the complete testbed are shown in Fig. 2. The multiuser CAP-MIMO testbed represents a versatile and novel platform for: i) multi-beam communication and sensing that is not possible with any other existing system, and at unprecedented spatial resolutions, and ii) development and real-time testing of new beam-frequency PHY and PHY-MAC protocols. We report initial results to illustrate both capabilities.

3 BEAMSPACE MIMO BASICS

An antenna aperture can be equivalently represented by its half-wavelength sampled version without any loss of information [1, 2]. The number of samples, n, represents the dimension of the two-dimensional (2D) spatial signal space and also determines the directivity or beamforming gain:

$$n = \frac{4A}{\lambda^2} = \frac{\pi D_{lens}^2}{\lambda^2} = 636\ ,\ G = 10\log_{10}(\pi n) = 33\text{dBi} \qquad (1)$$

where A is the area of the antenna aperture and the numerical values are for the prototype with lens diameter $D_{lens} = 6$" at 28 GHz. Thus, the prototype lens aperture is equivalent to a half-wavelength spaced 2D array with 636 elements.

3.1 Antenna Domain System Modeling

Consider communication from a single MS to a CAP-MIMO AP. The baseband system equation in aperture-frequency domain is given by

$$\boldsymbol{r}(f) = \boldsymbol{h}(f)x(f) + \boldsymbol{w}(f)\ ,\ -W/2 \le f \le W/2 \qquad (2)$$

where $\boldsymbol{r}(f)$ is the $n \times 1$ vector of received frequency domain signals on the critical samples of the antenna aperture, $\boldsymbol{h}(f)$ is the $n \times 1$ vector of aperture-domain frequency responses from the MS to the AP, $x(f)$ is the transmitted frequency-domain signal from the MS, and $\boldsymbol{w}(f)$ is the $n \times 1$ noise vector in the frequency domain with power spectral density (PSD) N_o. The noise at distinct sampled aperture elements is assumed to be independent.

In general, the aperture-domain vector of channel frequency responses can be modeled as

$$\boldsymbol{h}(f) = \sum_{\ell=0}^{N_p} \beta_\ell \boldsymbol{a}_n(\theta_\ell) e^{-j2\pi\tau_\ell f} \qquad (3)$$

where β_ℓ is the complex path attenuation, τ_ℓ is the path delay, and $\theta_\ell = (\theta_{az,\ell}, \theta_{el,\ell}) \in [-0.5, 0.5] \times [-0.5, 0.5]$ is the pair of spatial

frequencies (normalized angles) in azimuth and elevation associated with the ℓ-th path. N_p denotes the total number of paths and the $\ell = 0$ path denotes the LoS path. We note that in this model, $\{\tau_\ell\}$ are all relative to the delay of the LoS (or strongest) path which we assume to be $\tau_0 = 0$ without loss of generality. The spatial frequencies $\theta = (\theta_{az}, \theta_{el})$ are related to the physical azimuth and elevation angles, $\phi = (\phi_{az}, \phi_{el}) \in [-\pi/2, \pi/2] \times [-\pi/2, \pi/2]$, as [2, 13]

$$\theta_{az} = \frac{1}{2}\sin(\phi_{az})\ ,\ \theta_{el} = \frac{1}{2}\sin(\phi_{el})\ . \tag{4}$$

In (3), $\boldsymbol{a}_n(\theta)$ represents the array response vector for a far-field point source in the direction $\theta \leftrightarrow \phi$. For uniform linear arrays (ULAs), $\boldsymbol{a}_n(\theta)$ takes the form of a discrete spatial sinusoid with frequency θ, and for critically sampled 2D uniform planar arrays (UPAs), $\boldsymbol{a}_n(\theta)$ is the kronecker product of the steering vectors of ULAs in azimuth and elevation [4]: $\boldsymbol{a}_n(\theta) = \boldsymbol{a}_{n_{az}}(\theta_{az}) \otimes \boldsymbol{a}_{n_{el}}(\theta_{el})$, where n_{az} and n_{el} are the array dimensions in azimuth and elevation and $n = n_{az} \times n_{el}$.

3.2 Beamspace MIMO System Modeling

In beamspace MIMO framework, the system is equivalently represented in the beamspace domain and the two are related through a spatial Fourier transform [2, 11, 13, 15, 16]. The (crtically sampled) beamspace domain is related to the aperture domain through a 2D Discrete Fourier Transform (DFT). Let $\boldsymbol{U}_n$ represent the $n \times n$ 2D DFT matrix whose columns consist of $\{\frac{1}{\sqrt{n}}\boldsymbol{a}_n(\theta_i)\}$ representing n orthogonal beam directions $\theta_i = i\Delta\theta = \frac{i}{n}$ with spacing $\Delta\theta = \frac{1}{n}$ [2, 11]. The beamspace signal representation is given by

$$\boldsymbol{x}_b(f) = \boldsymbol{U}_n^H \boldsymbol{x}(f) \Longleftrightarrow \boldsymbol{x}(f) = \boldsymbol{U}_n \boldsymbol{x}_b(f)\ . \tag{5}$$

The beam-frequency domain representation of the baseband system equation in (2) is

$$\boldsymbol{r}_b(f) = \boldsymbol{U}_n^H \boldsymbol{r}(f) = \boldsymbol{h}_b(f)x(f) + \boldsymbol{w}_b(f) \tag{6}$$

$$\boldsymbol{h}_b^H = \boldsymbol{U}_n^H \boldsymbol{h}(f)\ ,\ \boldsymbol{w}_b(f) = \boldsymbol{U}_n^H \boldsymbol{w}(f) \tag{7}$$

where $\boldsymbol{r}_b(f)$ is the $n \times 1$ vector of received frequency domain signal in the beamspace domain, $\boldsymbol{h}_b(f)$ is the $n \times 1$ vector of beamspace frequency responses from the MS to each of the AP feed antennas, and $\boldsymbol{w}_b(f)$ is the $n \times 1$ noise vector with PSD N_o. The critically-sampled aperture domain and beamspace domain representations are equivalent since $\boldsymbol{U}_n$ is a unitary matrix: $\boldsymbol{U}_n^H \boldsymbol{U}_n = \boldsymbol{U}_n \boldsymbol{U}_n^H = \boldsymbol{I}$. As a result, the noise in different beams is also independent.

For 2D UPAs the unitary beamforming matrix $\boldsymbol{U}_n$ for mapping the aperture domain into the beamspace domain is given by: $\boldsymbol{U}_n = \boldsymbol{U}_{n_{az}} \otimes \boldsymbol{U}_{n_{el}}$. Using (3), the beamspace channel frequency response vector $\boldsymbol{h}_b(f) = \boldsymbol{U}_n^H \boldsymbol{h}(f)$ is given by

$$\boldsymbol{h}_b(f) = \sum_{\ell=0}^{N_p} \beta_\ell \boldsymbol{U}_{n_{az}}^H \boldsymbol{a}_{n_{az}}(\theta_{az,\ell}) \otimes \boldsymbol{U}_{n_{el}}^H \boldsymbol{a}_{n_{el}}(\theta_{el,\ell}) e^{-j2\pi\tau_\ell f} \tag{8}$$

Specifically, the element of $\boldsymbol{h}_b(f)$ corresponding to the i-th fixed angle in azimuth and k-th fixed angle in elevation is

$$\begin{aligned} h_{b,i,k}(f) &= \frac{1}{\sqrt{n}} \sum_{\ell=0}^{N_p} \beta_\ell f_{n_{az}}\left(\theta_{az,\ell} - \frac{i}{n_{az}}\right) \\ &= f_{n_{el}}\left(\theta_{el,\ell} - \frac{k}{n_{el}}\right) e^{-j2\pi\tau_\ell f} \end{aligned} \tag{9}$$

where $f_n(\theta) = \sin(n\pi\theta)/\sin(\pi\theta)$ is the Dirichlet sinc function with a peak of n at $\theta = 0$ and zeros at multiples of $1/n$. The corresponding impulse response is given by

$$\begin{aligned} g_{b,i,k}(\tau) = \frac{1}{\sqrt{n}} \sum_{\ell=0}^{N_p} \beta_\ell f_{n_{az}}\left(\theta_{az,\ell} - \frac{i}{n_{az}}\right) \\ f_{n_{el}}\left(\theta_{el,\ell} - \frac{k}{n_{el}}\right) \mathrm{sinc}\left(W\left(\tau - \frac{\tau_\ell}{W}\right)\right) \end{aligned} \tag{10}$$

where $\mathrm{sinc}(x) = \sin(\pi x)/(\pi x)$ is the sinc function. The relationship (10) states that $g_{b,i,k}(\tau)$ is peaky in the path beam directions $(\theta_{az,\ell}, \theta_{el,\ell})$ and delays τ_ℓ. Furthermore, $g_{b,i,k}(\tau)$ exhibits sparse peaks in angle-delay due to primarily LoS and single-bounce multipath propagation since multiple bounces incur significant attenuation at mmW frequencies.

3.3 CAP-MIMO: Beamspace Through a Lens Array

In CAP-MIMO, the front-end lens array computes an approximate 2D Fourier transform of the aperture domain signal $\boldsymbol{r}(f)$, and the elements of the beamspace signal vector $\boldsymbol{r}_b(f)$ are obtained by critically sampling the focal surface of the lens [2, 11]. Critical sampling in beamspace is related to the angular beamwidth which is approximately given by [2, 11]

$$\Delta\phi = \frac{\lambda}{D_{lens}}\ \text{(radians)} \tag{11}$$

and is about 4^o for a 6" lens at 28 GHz. The current CAP-MIMO prototype samples the focal surface with a 4×4 16-element array centered on broadside, see Fig. 1(b) and 1(d), spanning an angular spread of about $\Delta\phi = 16^o$ in both elevation and azimuth. A larger angular spread can be covered by either moving the 16-element array along the focal surface or by using a larger feed array.

4 SIGNALING FRAME AND RECEIVER PROCESSING

The BPUs of the CAP-MIMO testbed can generate arbitrary waveforms for communication and sensing. We illustrate initial results using Orthogonal Frequency Division Multiplexing (OFDM) waveforms with $N = 256$ tones. The sampling interval and the OFDM symbol duration are

$$T_s = \frac{1}{W} = 2.7\text{ns and } T_{ofdm} = NT_s = 0.7\mu\text{s}\ . \tag{12}$$

The transmission frame is shown in Fig. 3 for multiuser communication from two MSs to the CAP-MIMO AP. The frame consists of the following blocks for each MS:

- **Beam Selection (BS)**: For selecting the strong beams.

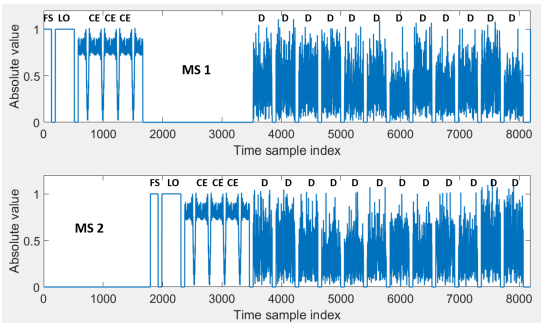

Figure 3: The transmission frame structure for two MSs

.

- **Frame Synchronization (FS)**: For time synchronization of the frame symbols.
- **Local Oscillator (LO) Offset Estimation**: For frequency synchronization with the AP.
- **Channel Estimation (CE)**: For estimating the channel frequency response for the selected beams.
- **Data (D)**: Data symbols.

A beacon signal transmitted from the AP initiates transmission from the MSs, a given time interval after reception of the beacon. The first part of the frame signal is for BS (not show in Fig. 3) in which the two MSs transmit in non-overlapping time intervals (similar to the FS/LO/CE blocks in Fig. 3). The BS signals are used for determining the strongest beams (with highest power) for each MS. Then four beams – one in each quadrant (see Fig. 1(d)) – and representing the two strongest beams from each MS are selected for joint beam-frequency processing of the received data signals at the AP.

Following BS, the two MSs transmit the frame as shown in Fig. 3 and AP collects the received signal on the selected beams [3]. The FS/LO/CE transmitted signals are known at the AP to enable time-frequency synchronization and channel estimation. The beam-frequency channel estimates for the two MSs are used for spatio-temporal equalization and interference suppression at the AP in the data blocks in which all MSs transmit simultaneously.

After time-frequency synchronization, the complex baseband system equation in beam-frequency for multiuser communication between K MSs, and a CAP-MIMO AP, is

$$\boldsymbol{r}_b(f) = \sum_{i=1}^{K} \boldsymbol{h}_{b,i}(f) x_i(f) + \boldsymbol{w}_b(f)\,,\ -W/2 \le f \le W/2 \qquad (13)$$

where $\boldsymbol{r}_b(f)$, $\boldsymbol{h}_{b,i}(f)$ and $\boldsymbol{w}_b(f)$ represent $N_b \times 1$ vectors of received frequency-domain signals for the $N_b = 16$ beamspace feed antennas; $\boldsymbol{h}_{b,i}(f)$ and $x_i(f)$ are the channel frequency response vector and the transmitted signal for the i-th user. OFDM signaling results in a frequency-domain sampled representation of the system equation in (6) with $\Delta f = \frac{W}{N} = 1.45$ MHz:

$$\boldsymbol{r}_b[k] = \sum_{i=1}^{K} \boldsymbol{h}_{b,i}[k] x_i[k] + \boldsymbol{w}_b[k]\,, \qquad (14)$$

where $\boldsymbol{r}_b[k] = \boldsymbol{r}_b(k\Delta f), k = -\frac{N}{2}, \cdots, 0, \cdots, \frac{N}{2} - 1$, is the sampled version of the received frequency-domain signal vector, and $\boldsymbol{w}_b[k]$, $\boldsymbol{h}_{b,i}[k]$ and $x_i[k]$, are defined similarly for the noise vector, the channel frequency response vectors and transmitted symbols.

5 MEASUREMENT RESULTS

Due to its discrete architecture, the CAP-MIMO testbed provides full access to mmW and baseband signal measurements. While direct measurements in the passband and baseband would require corresponding instrumentation (e.g. an oscilloscope with sufficiently large bandwidth), the BPU provides baseband measurements at sampling rates and bit resolution afforded by the ADCs. We are developing the FPGA-based BPU for both *real-time* testing of wideband multi-beam communication and sensing protocols, as well as collection of raw beam-frequency measurements for *offline* processing and analysis. In this section, we present results based on initial measurements. The MSs served as the transmitters, and for a given location of the MSs and the AP, $M = 100$ measurements, $\boldsymbol{r}_b^m[k]$, $m = 1, \cdots, M$, of the received signal vector $\boldsymbol{r}_b[k]$ were taken for M frame transmissions from the MSs. The measurement were then processed to illustrate three aspects of the testbed: i) directional focusing by a lens array, ii) multiuser communication between multiple MSs and the CAP-MIMO AP, and iii) beam-frequency channel measurements, processing, and analysis.

5.1 Outdoor Directional LoS Measurements

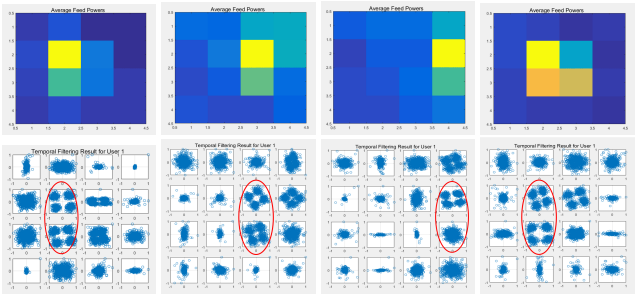

Figure 4: Feed array powers and processed received signals for an outdoor LoS link of length 154 ft. (a) MS in broadside direction. (b) MS 11 ft to the left of broadside. (c) MS 22 ft to the left of broadside. (d) MS 22 ft to the left and the feed array moved correspondingly.

The first set of results illustrate the directional focusing of the lens antenna array in an outdoor LoS link of length 154 feet between a single-antenna MS transmitter and the CAP-MIMO AP receiver. Fig. 4 shows the image of the relative powers in the feed array (top row) and the corresponding processed received (I/Q) data signals (bottom row) for four different link configurations. In Fig. 4(a), the MS is in the broadside direction of the CAP-MIMO AP. In Fig. 4(b), the MS is moved 11 feet (one beamwidth at 154 feet link length) to the left, and in Fig. 4(c) 22 feet to the left, relative to broadside. In Fig. 4(d), the MS is still 22 feet to the left but the feed array is moved in the opposite direction on the focal surface by a corresponding amount (twice the orthogonal feed spacing). As expected, the position of strong feeds tracks the MS as expected, and only the signals in the few (1-3) strong feeds surrounding the MS location can be reliably decoded.

5.2 Indoor Multiuser Hallway Measurements

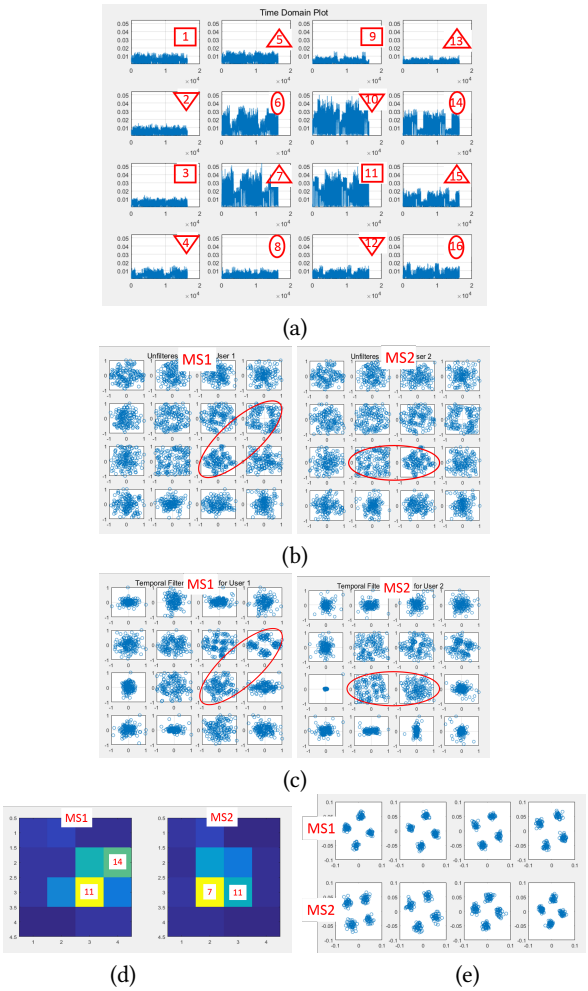

Figure 5: Multiuser processing of two MSs separated by 3 feet and at a distance of 28.5 feet from the CAP-MIMO AP. (a) Received time-domain frame signals for all 16 feeds. (b) Unprocessed frequency domain data signals. (c) Temporally processed frequency domain data signals. (d) Received feed powers for the two MSs, with the selected beams labeled. (e) Spatially combined (over selected beams) and temporally filtered signals for four data blocks.

Fig. 5 shows results for indoor hallway measurements between two MSs separated by 3 feet (about 1.5 times the beamwidth) and at a distance of 28.5 feet from the CAP-MIMO AP. The hallway had a width of 8 feet, height of 9 feet, and a length of 95 feet. Fig. 5(a) shows the received temporal frame signals for all 16 feeds (corresponding to the transmit frame signal in Fig. 3); see (14). The feeds with the same marker (e.g., 1, 9, 3, 11) were measured simultaneously through the four RF chains for a given setting of switches; see also Fig. 1(d). Fig. 5(b) shows the unprocessed frequency domain *data* signals for the two MSs for all the 16 feeds (extracted from $\boldsymbol{r}_b[k]$ after time synchronization; frequency synchronization was not needed since LO offset was very small). The two strongest beams for each MS are circled. Fig. 5(c) shows the data signals for all feeds for both MSs after frequency-domain equalization. As can be seen, the QAM symbols for feed 14 of MS 1 are well separated; the symbols in neither of the two strong beams for MS 2 are well-separated. Fig. 5(d) shows the feed powers for the two MSs' training signals, and the strongest beams are labeled and correspond to those in Figs. 5(b)-(c). Finally, Fig. 5(e) shows the signals for four consecutive data blocks for each MS after spatial combining and frequency-domain equalization of the four selected feeds [3, 13]. The QAM constellations for both MSs are well separated. This demonstrates the ability of CAP-MIMO to separate the signals of two closely located MSs through appropriate spatial interference suppression and temporal equalization; temporal processing alone is unable to decode the signals as evident from Figs. 5(b)-(c).

5.3 Channel and System Data Analysis

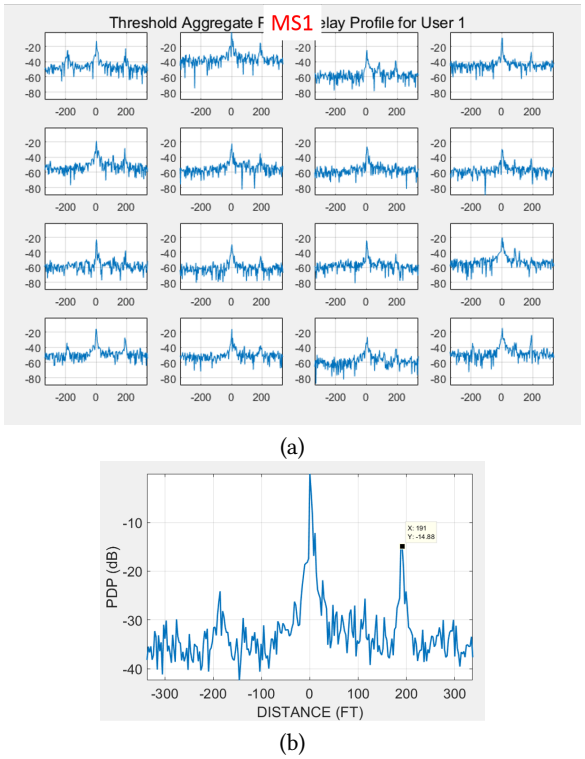

Figure 6: PDP for MS 1 for the MU hallway measurements. (a) PDPs for individual beams. (b) Aggregated PDP over all beams.

Finally, we illustrate processing of beam-frequency channel measurements to generate channel power delay profiles (PDPs). For a given location of the MSs, the $M = 100$ measurements, $\boldsymbol{r}_b^m[k]$, $m = 1, \cdots, M$, of the received signal vector, $\boldsymbol{r}_b[k]$, were processed in MATLAB to extract $M = 100$ channel beam-frequency response vectors $\boldsymbol{h}_b^m[k]$, which were then averaged to yield a 16×1 *average beam-frequency response vector* for each MS:

$$\bar{\boldsymbol{h}}_b[k] = \frac{1}{M}\sum_{m=1}^{M} \boldsymbol{h}_b^m[k] = \left[\bar{h}_{b,1}[k], \cdots, \bar{h}_{b,N_b}[k]\right]^T \qquad (15)$$

where $\bar{h}_{b,i}[k] = \bar{h}_{b,i}(k\Delta f)$, $k = -\frac{N}{2}, \cdots, 0, \cdots, \frac{N}{2} - 1$, represents the k-th sample of the average frequency response for the i-th beam. The beam-impulse response vectors, $\boldsymbol{g}_b^m[n]$, are obtained from $\boldsymbol{h}_b^m[k]$ through an N-point FFT operation, and the corresponding *average channel impulse response vectors* are given by

$$\bar{\boldsymbol{g}}_b[n] = \left[\bar{g}_{b,1}(n), \cdots, \bar{g}_{b,N_b}[n]\right]^T \ , \ n = 0, \cdots, N-1 \qquad (16)$$

where $\bar{g}_{b,i}[n] = \bar{g}_{b,i}(nT_s)$ is the sampled version of the averaged impulse response for the i-th beam/channel; see (10).

The average power spectral density (PSD) and the average path delay profile (PDP) for the i-th beam are calculated as

$$\text{PSD}_i[k] = |\bar{h}_{b,i}[k]|^2 \ , \ \text{PDP}_i[n] = |\bar{g}_{b,i}[n]|^2 \qquad (17)$$

and represent the distribution of channel power in beam-frequency or beam-delay, respectively. The *aggregate* PSD and the *aggregate* PDP (over all beams) are given by

$$\text{PSD}[k] = \sum_{i=1}^{N_b} \text{PSD}_i[k] \ , \ \text{PDP}[n] = \sum_{i=1}^{N_b} \text{PDP}_i[n] \ . \qquad (18)$$

Fig. 6 shows the PDPs for MS 1 for the hallway measurements discussed in Sec. 5.2. Fig. 6(a) shows the PDPs for each of the $N_b = 16$ beams; note that the middle four beams are the strongest. Fig. 6(b) shows the aggregate PDP over all beams; see (18). A significant multipath reflection (-15dB below LoS) at a distance of 200 feet relative to the LoS path is noted. This corresponds to twice the roundtrip time between the end walls of the hallway which is 95 feet long. We note that there is a metal door frame on one end of the hallway.

6 CONCLUDING REMARKS

In this paper we have outlined a new multi-beam methodology for mmW MIMO experimentation and channel measurements, and presented initial results using measurements from a 28 GHz CAP-MIMO prototype testbed. We have reported new results that showcase the capabilities of the multi-beam MIMO testbed in three aspects: directional communication, multiuser processing, and channel data analytics. The multi-beam CAP-MIMO testbed opens new possibilities for mmW communication, sensing and measurements that are not possible with existing systems. Two aspects are particularly noteworthy. First, it enables unprecedented spatial resolutions; e.g., the spatial resolution of the current CAP-MIMO prototype is comparable to a conventional 2D array with over 600 half-wavelength-spaced elements. Second, simultaneous multi-beam measurements enable new capabilities, including measurement of second- and higher-order channel statistics, and synchronization of multiple measurements. Our near-term goal is to develop a testbed network consisting of four CAP-MIMO AP nodes and four MS nodes.

There are several aspects in which we are further developing the mmW CAP-MIMO testbed. First, we are developing a basic set of PHY-MAC protocols for real-time experimentation. Second, we are extending the mmW hardware to enable bi-directional operation. Third, we are developing a computational framework for offline processing and analysis of measurement data for a variety of aspects, including trouble shooting of protocols implemented on the testbed and leveraging channel measurement traces, channel statistics and models for link-level and network-level simulation. We plan to share all critical design specifications of the testbed with the wider mmW academic research community to facilitate its replication at other institutions for further research and technology development. In particular, we are very interested in conducting a comprehensive comparison of phased arrays and lens array from the viewpoint of critical metrics, such as performance, cost, and complexity in different use cases.

Additional work is also needed for calibrating and optimizing the testbed. As in any hardware system, the testbed measurements represent a combination of the true underlying propagation environment as well as the intrinsic beam-frequency response of the hardware, including the lens array. Using a Vector Network Analyzer to measure the beam-frequency response of the CAP-MIMO mmW hardware can be utilized for this calibration. There are also several aspects in which the lens array design can be optimized for different use cases and performance metrics.

REFERENCES

[1] C. A. Balanis. 1997. *Antenna Theory: Analysis and Design.* Wiley-New York.

[2] J. Brady, N. Behdad, and A. Sayeed. 2013. Beamspace MIMO for Millimeter-wave Communications: System Architecture, Modeling, Analysis and Measurements. *IEEE Transactions on Antenna and Propagation* (July 2013), 3814–3827.

[3] J. Brady, J. Hogan, and A. Sayeed. 2016. Multi-Beam MIMO Prototype for Real-Time Multiuser Communication at 28 GHz. *IEEE Globecom Workshop on Emerging Technologies for 5G* (Dec. 2016).

[4] J. W. Brewer. 1978. Kronecker Products and Matrix Calculus in System Theory. *IEEE Trans. Circ. and Syst.* 25, 9 (Sep. 1978), 772–781.

[5] A. Goldsmith. 2006. *Wireless Communications.* Cambridge University Press.

[6] R. W. Heath, N. González-Prelcic, S. Rangan, W. Roh, and A. M. Sayeed. 2016. An Overview of Signal Processing Techniques for Millimeter Wave MIMO Systems. *IEEE Journal of Selected Topics in Signal Processing* 10, 3 (April 2016), 436–453.

[7] S. Hur, Y.-J. Cho, T. Kim, J. Park, A. Molisch, K. Haneda, and M. Peter. 2015. Wideband spatial channel model in an urban cellular environments at 28 GHz. In *Antennas and Propagation (EuCAP), 2015 9th European Conference on.* 1–5.

[8] G. R. Maccartney, T. S. Rappaport, S. Sun, and S. Deng. 2015. Indoor Office Wideband Millimeter-Wave Propagation Measurements and Channel Models at 28 and 73 GHz for Ultra-Dense 5G Wireless Networks. *IEEE Access* 3 (2015), 2388–2424.

[9] Z. Pi and F. Khan. 2011. An Introduction to Millmeter-Wave Mobile Broadband Systems. *IEEE Commununications Magazine* (June 2011), 101–107.

[10] T.S. Rappaport, Shu Sun, R. Mayzus, Hang Zhao, Y. Azar, K. Wang, G.N. Wong, J.K. Schulz, M. Samimi, and F. Gutierrez. 2013. Millimeter Wave Mobile Communications for 5G Cellular: It Will Work! *Access, IEEE* 1 (2013), 335–349.

[11] A. Sayeed and N. Behdad. 2010. Continuous Aperture Phased MIMO: Basic Theory and Applicatons. *Proc. 2010 Annual Allerton Conference on Communications, Control and Computers* (Sep. 2010), 1196–1203.

[12] A. Sayeed and J. Brady. 2016. Beamspace MIMO Channel Modeling and Measurement: Methodology and Results at 28 GHz. *IEEE Globecom Workshop on Millimeter-Wave Channel Modeling* (Dec. 2016).

[13] A. Sayeed and J. Brady. 2016. *Millimeter-Wave MIMO Transceivers: Theory, Design and Implementation.* Signal Processing for 5G: Algorithms and Implementations (F.-L. Luo and J. Zhang, Eds.), IEEE-Wiley.

[14] A. Sayeed, J. Brady, P. Cheng, and U. Tayyab. 2016. Indoor Channel Measurements Using a 28 GHz Multi-beam MIMO Prototype. *IEEE Vehicular Technology Conference Workshop on Millimeter-Wave Channel Models,* (Sep. 2016).

[15] A. Sayeed and T. Sivanadyan. 2010. *Wireless Communication and Sensing in Multipath Environments using Multi-antenna Transceivers.* Handbook on Array Processing and Sensor Networks (K. J. R. Liu and S. Haykin, Eds.), IEEE-Wiley.

[16] A. M. Sayeed. 2002. Deconstructing Multi-Antenna Fading Channels. *IEEE Trans. Signal Processing* 50, 10 (Oct. 2002), 2563–2579.

[17] 5G Channel Modeling SIG. 2016. 5G Channel Model for Bands Up to 100 GHz. *White Paper* (Oct. 2016).

[18] A. L. Swindlehurst, E. Ayanoglu, P. Heydari, and F. Capolino. 2014. Millimeter-wave massive MIMO: the next wireless revolution? *IEEE Communications Magazine* 52, 9 (Sep. 2014), 56–62.